

Design of Multilevel Reed–Solomon Codes and Iterative Decoding for Visible Light Communication

Xin Huang, Li Chen¹, Senior Member, IEEE, Wenjun Chen¹, and Ming Jiang¹, Senior Member, IEEE

Abstract—This paper proposes multilevel Reed–Solomon (MRS) codes and their iterative multistage soft decoding (IMSD) for visible light communication (VLC), realizing both high decoding performance and transmission spectrum efficiency. The proposed IMSD algorithm decodes the MRS codes level-by-level through iterating either hard decisions or extrinsic information of RS coded bits. Each level RS decoding is realized by cascading the adaptive belief propagation (ABP) algorithm that produces the extrinsic information and the Berlekamp–Massey (BM) algorithm that estimates the codeword. The earlier level decoding provides better *a priori* information for the later ones. A complexity reducing IMSD (CR-IMSD) algorithm is also proposed to facilitate the decoding. This paper further investigates a joint design of color-shift keying (CSK) constellation and the MRS code, optimizing the decoding performance. The CSK constellation is designed by considering both the set partitioning (SP) criterion and the harmonic mean of constellation’s minimum squared Euclidean distance (MSED). The MRS codes are further designed using the capacity and the equal error probability rules. Our simulation results show that the IMSD algorithm achieves significant iterative decoding gains. The performance of the designed MRS code is 0.3 dB away from the capacity limit at the bit error rate (BER) of 10^{-9} .

Index Terms—Color-shift keying, iterative multistage soft decoding, multilevel Reed–Solomon codes, visible light communication.

I. INTRODUCTION

VISIBLE light communication (VLC) [1], [2] has emerged to overcome the spectrum shortage in radio frequency communication. It provides extra unregulated bandwidth resources and high rate downlink communication. Conveying information using the low cost and energy efficient light emitting diodes (LEDs), VLC is prospective in many scenarios, especially indoor communication.

Color-shift keying (CSK) is designed for VLC to realize high transmission spectrum efficiency and easy dimming

Manuscript received June 16, 2018; revised October 24, 2018 and January 23, 2019; accepted March 1, 2019. Date of publication March 12, 2019; date of current version July 13, 2019. This work is supported by the National Natural Science Foundation of China (NSFC) with project ID 61671486 and 61771499. This paper was presented in part at the 2018 IEEE Information Theory Workshop (ITW) with the article titled “Iterative Multistage Soft Decoding of Multilevel Reed–Solomon Codes.” The associate editor coordinating the review of this paper and approving it for publication was H. Saeedi. (Corresponding author: Li Chen.)

X. Huang, W. Chen, and M. Jiang are with the School of Electronics and Information Technology, Sun Yat-sen University, Guangzhou 510006, China (e-mail: huangx259@mail2.sysu.edu.cn; chenwj47@mail2.sysu.edu.cn; jiangm7@mail.sysu.edu.cn).

L. Chen is with the School of Electronics and Communication Engineering, Sun Yat-sen University, Guangzhou 510006, China (e-mail: chenli55@mail.sysu.edu.cn).

Color versions of one or more of the figures in this paper are available online at <http://ieeexplore.ieee.org>.

Digital Object Identifier 10.1109/TCOMM.2019.2904563

support [3]. CSK constellation optimization has been considered in [4]–[7]. The quad-chromatic LED (QLED) CSK modulation has been proposed to achieve a significant performance improvement over the trichromatic LED (TLED) [8], [9]. A hybrid CSK system, for instance the one combining CSK with spatial modulation, has been also proposed in [10]. However, channel coding has not been employed in the above research. In order to further achieve reliable VLC, Reed–Solomon (RS) codes, convolutional codes and turbo codes using CSK modulation have been considered in [11]–[15]. To facilitate the iterative decoding performance, a CSK design based on the extrinsic information transfer (EXIT) characteristics has been conceived in [14]. Moreover, a hierarchical CSK constellation has been designed for video streaming, realizing unequal error protection [11]. Integrating multiple error-correction codes with a high-order modulation, multilevel coding [16] can further achieve both high decoding performance and spectrum efficiency. The error-correction codes are called the component codes. The corresponding coded bits of each component code are grouped and mapped to a constellation symbol for transmission. However, multilevel coding has not been considered for VLC which is equipped with a high-order CSK modulation. It is also unknown how to design CSK constellations for multilevel coding.

The multilevel coding scheme allows its component codes to be decoded one-by-one, resulting in a level-by-level message recovery mechanism. Consequently, later decoding events benefit from the earlier ones. To fully exploit the decoding potential, iterative multistage soft decoding (IMSD) of multilevel codes has been proposed by Martin and Taylor [17] and Isaka and Imai [18], respectively. With the iterative decoding, multilevel code design using the EXIT function has been considered in [19]. However, the VLC standard code, i.e., the RS code [3], has not been considered as component codes for multilevel codes in the above work. RS codes are nonbinary maximum distance separable codes. They have a competent burst error-correction capability. Using the Berlekamp–Massey (BM) algorithm [20], it can correct errors up to half of the code’s minimum Hamming distance. Applications of multilevel RS (MRS) codes have been considered by Husni [21], Husni and Sweeney [22], and Chung and Lou [23], respectively. However, these existing decoding algorithms for MRS codes are hard-decision oriented with limited error-correction performance. The IMSD for MRS codes has not been developed due to the high complexity of realizing RS soft-in soft-out (SISO) decoding. The early bit level soft-decision decoding of RS codes was proposed by Vardy and Be’ery [24]. Ponnampalam and Vucetic [25] proposed the

maximum *a posteriori* probability (MAP) decoding of RS codes, realizing the RS SISO decoding. However, the number of trellis states of a RS code grows exponentially with the number of its parity symbols where the finite field size is the base, implying SISO decoding of long RS codes infeasible. Jiang and Narayanan [26] proposed the adaptive belief propagation (ABP) decoding of RS codes where the decoding exhibits a polynomial-time complexity. This makes SISO decoding of RS codes more practical. This paper further applies the ABP algorithm in decoding of each component code of an MRS code, generating both the extrinsic and the *a posteriori* probabilities of RS coded bits. Iterating with demapping, it forms a novel IMSD algorithm for MRS codes. Contributions of the paper can be outlined as follows.

- We propose an IMSD algorithm for MRS codes. Each level RS SISO decoding is realized by cascading the ABP algorithm and the BM algorithm. The ABP algorithm produces both the extrinsic and the *a posteriori* information for RS coded bits. The BM algorithm decodes the codeword using the decisions made based on the *a posteriori* information provided by the ABP algorithm. In the multistage decoding mechanism, the earlier level decoding events facilitate the later ones by providing a better *a priori* information. Iterating the extrinsic information of RS coded bits, the IMSD algorithm is able to achieve remarkable iterative decoding gains.
- A complexity reducing IMSD (CR-IMSD) algorithm is also proposed to facilitate the decoding. It reduces the ABP decoding latency by decreasing the number of the Gaussian eliminations. Our simulation results will further show its performance-complexity tradeoff, demonstrating its practical merit.
- A joint design of CSK constellation and MRS code under the IMSD paradigm is carried out. The CSK constellation is designed by considering both the set partitioning (SP) criterion and the harmonic mean of constellation's minimum squared Euclidean distance (MSED). We further investigate the code design of MRS codes using different approaches, including the capacity rule, the equal error probability rule and the balanced distances rule. They lead to heterogeneous multilevel codes, providing unequal error protection for different levels. Using the capacity rule, the designed MRS code is 0.3 dB away from the capacity limit at the bit error rate (BER) of 10^{-9} .

The rest of the paper is organized as follows. Section II presents the background knowledge for the paper. Section III proposes the IMSD algorithm and its complexity reducing variant. Section IV considers a joint design of CSK constellation and MRS code. Section V shows our simulation results. Finally, Section VI concludes the paper.

II. BACKGROUND KNOWLEDGE

This section provides the background knowledge of the paper, including CSK modulation and MRS codes.

A. CSK Modulation

For an M -CSK modulation, every m bits are mapped to a CSK symbol, where $m = \log_2 M$. Fig. 1 shows the

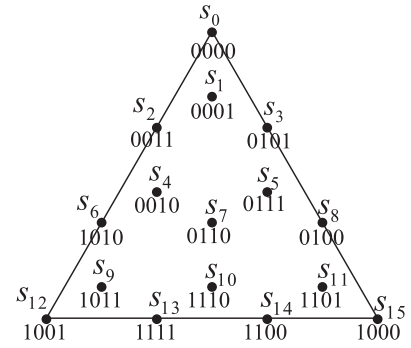


Fig. 1. The 2D projection of the IEEE standard 16-CSK constellation in intensity domain.

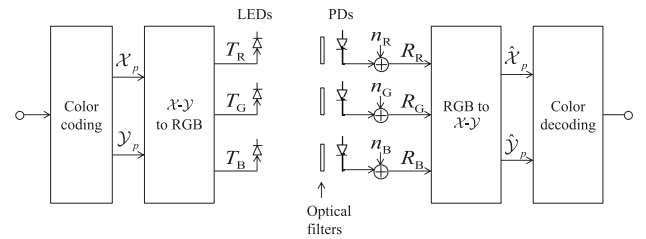


Fig. 2. The transceiver structure of M -CSK.

two dimensional (2D) projection of a 16-CSK constellation in intensity domain and its corresponding labeling strategy, which is specified in the IEEE standard [3]. For an M -ary CSK constellation $\mathcal{S} = \{s_0, s_1, \dots, s_{M-1}\}$, its symbol s_i ($i = 0, 1, \dots, M-1$) can be described as a three dimensional vector. That says, s_i can be represented by $[T_R, T_G, T_B]$, where T_R , T_G and T_B are the red, green and blue (RGB) intensity components of the LED transmitters, respectively. Nine different color band combinations (CBCs) based on different choices on frequencies of RGB lights are introduced in [3]. Our work is based on CBC-1 due to the fact that the minimum Euclidean distances (MED) of the constellations in intensity domain are identical for different CBCs [8].

Fig. 2 shows the transceiver structure of M -CSK. Let $(\mathcal{X}_R, \mathcal{Y}_R)$, $(\mathcal{X}_G, \mathcal{Y}_G)$ and $(\mathcal{X}_B, \mathcal{Y}_B)$ denote the chromaticity values at the central wavelengths of RGB LEDs, respectively. For M -CSK, every m bits are mapped to the $\mathcal{X}\mathcal{Y}$ chromaticity coordinate by color coding, resulting in the chromaticity value $(\mathcal{X}_p, \mathcal{Y}_p)$. Then the $(\mathcal{X}_p, \mathcal{Y}_p)$ is converted into the intensity vector $[T_R, T_G, T_B]$ by the following one-to-one linear mapping

$$\begin{cases} \mathcal{X}_p = T_R \mathcal{X}_R + T_G \mathcal{X}_G + T_B \mathcal{X}_B \\ \mathcal{Y}_p = T_R \mathcal{Y}_R + T_G \mathcal{Y}_G + T_B \mathcal{Y}_B \\ T_R + T_G + T_B = 1 \end{cases} \quad (1)$$

The transmitted intensity is kept constant to eliminate the flickering of LEDs, ensuring the normal illumination function.

The generated optical intensity signals are then emitted by the RGB LEDs. They propagate through the optical channel to the photodetectors (PDs). Generally speaking, in a simplified indoor VLC scenario a good portion of the received signal power comes from the line-of-sight (LOS) component, while

other components such as diffusion, multipath propagation and dispersion may be considered as marginal. Therefore, we can adopt the additive white Gaussian noise (AWGN) channel model where the channel interference is characterized by the additive noise [14]. Let R_R , R_G , R_B denote the intensity outputs at each PD, respectively. Consequently, the received intensities can be represented by

$$\begin{cases} R_R = T_R + n_R \\ R_G = T_G + n_G \\ R_B = T_B + n_B \end{cases} \quad (2)$$

where n_R , n_G , n_B are the AWGN imposed on the respective signals during the optical-electrical conversion at the PDs. Optical filters are required at the receivers to extract the intensities of each color channel and retrieve the chromaticities. The received chromaticity ($\hat{\mathcal{X}}_p, \hat{\mathcal{Y}}_p$) can be calculated based on R_R , R_G and R_B by using (1). Generally, the detection can be based on received intensities or chromaticities. The former is more popular since it yields a greater MED.

We now define the notations for the CSK constellations.

- Given an M -CSK constellation \mathcal{S} , its CSK symbol s_i is mapped from bits $[\theta_0, \theta_1, \dots, \theta_{m-1}]$, where $\theta_t \in \{0, 1\}$ and $t = 0, 1, \dots, m-1$. Let ϖ_i denote the decimal label of s_i , where $\varpi_i = \sum_{t=0}^{m-1} 2^{m-1-t} \cdot \theta_t$. E.g., in Fig. 1, the decimal labels of s_3 and s_5 are $\varpi_3 = 5$ and $\varpi_5 = 7$, respectively.
- Let $\mathcal{M}(\cdot)$ and $\mathcal{M}^{-1}(\cdot)$ denote the mapping and demapping functions, respectively. Based on the above definitions, we know that for M -CSK, $\mathcal{M}(\theta_0, \theta_1, \dots, \theta_{m-1}) = s_i$ and $\mathcal{M}^{-1}(s_i) = [\theta_0, \theta_1, \dots, \theta_{m-1}]$. We use $[\mathcal{M}^{-1}(s_i)]_t$ to denote bit t of the demapping. E.g., for the constellation in Fig. 1, $\mathcal{M}^{-1}(s_4) = 0010$ and $[\mathcal{M}^{-1}(s_4)]_2 = 1$. Moreover, we define $\mathcal{S}_{t,\theta} = \{s_i \mid [\mathcal{M}^{-1}(s_i)]_t = \theta \text{ and } s_i \in \mathcal{S}\}$ as the set of symbols whose demapping yields bit t being θ , where $\theta \in \{0, 1\}$. E.g., in Fig. 1, $\mathcal{S}_{1,0} = \{s_0, s_1, s_2, s_4, s_6, s_9, s_{12}, s_{15}\}$.

B. MRS Codes

Fig. 3 shows the structure of an MRS code. It integrates m RS codes with an M -CSK modulation, where RS codes are called component codes. Every m RS coded bits that come from the m component codes are mapped to an M -CSK symbol.

Let $\mathbb{F}_{2^p} = \{0, 1, \alpha^1, \alpha^2, \dots, \alpha^{2^p-2}\}$ denote a finite field of size 2^p , where p is a positive integer and α is a primitive element of the field. In an MRS coding scheme, an (n_t, k_t) RS code defined over \mathbb{F}_{2^p} is utilized at level t , where $n_t = 2^p - 1$ and k_t are the length and dimension of the code, respectively. Using the BM algorithm, it can correct at most $\lfloor \frac{n_t - k_t}{2} \rfloor$ symbol errors. Since the all the component codes should maintain the same length, we let $n_t = n$, $\forall t$. At level t , generator polynomial of the (n, k_t) RS code can be defined as

$$g_t(x) = (x - \alpha^1)(x - \alpha^2) \cdots (x - \alpha^{n-k_t}). \quad (3)$$

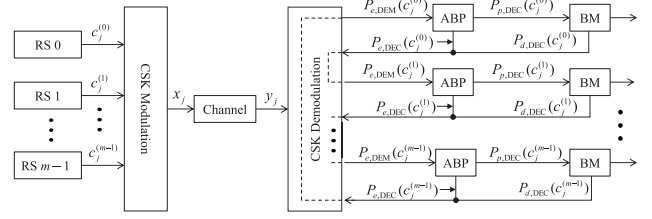


Fig. 3. MRS code and the IMSD scheme.

Given a message vector at level t as $\underline{U}^{(t)} = [U_0^{(t)}, U_1^{(t)}, \dots, U_{k_t-1}^{(t)}] \in \mathbb{F}_{2^p}^{k_t}$, its message polynomial $U^{(t)}(x)$ is

$$U^{(t)}(x) = U_0^{(t)} + U_1^{(t)}x + \cdots + U_{k_t-1}^{(t)}x^{k_t-1}. \quad (4)$$

The level- t RS codeword can be generated by

$$\begin{aligned} C^{(t)}(x) &= x^{n-k_t}U^{(t)}(x) + x^{n-k_t}U^{(t)}(x) \bmod g_t(x) \\ &= C_0^{(t)} + C_1^{(t)}x + \cdots + C_{n-1}^{(t)}x^{n-1}. \end{aligned} \quad (5)$$

The codeword vector is $\underline{C}^{(t)} = [C_0^{(t)}, C_1^{(t)}, \dots, C_{n-1}^{(t)}] \in \mathbb{F}_{2^p}^n$. For an MRS code, if $k_0 = k_1 = \dots = k_{m-1}$, all levels exhibit a homogeneous structure. It is therefore called the homogeneous MRS (HoMRS) code. Otherwise, It is called the heterogeneous MRS (HeMRS) code. Let

$$\mathcal{R}^{(t)} = \frac{k_t}{n} \quad (6)$$

denote the rate of the level- t RS code. The rate of the MRS code is defined as

$$\mathcal{R} = \frac{1}{m} \sum_{t=0}^{m-1} \mathcal{R}^{(t)}. \quad (7)$$

For HoMRS codes, $\mathcal{R}^{(t)} = \mathcal{R}$, $\forall t$.

In order to map the codewords into CSK symbols, each codeword $\underline{C}^{(t)}$ needs to be converted into its binary version $\underline{c}^{(t)} = [c_0^{(t)}, c_1^{(t)}, \dots, c_{n-1}^{(t)}]$. Then m RS coded bit sequences are mapped into M -CSK symbols by $x_j = \mathcal{M}(c_j^{(0)}, c_j^{(1)}, \dots, c_j^{(m-1)})$, resulting in the modulated symbol sequence $x_0, x_1, \dots, x_{np-1}$, where $x_j \in \mathcal{S}$ and $j = 0, 1, \dots, np-1$. After the channel, the received symbol sequence $y_0, y_1, \dots, y_{np-1}$ is obtained at the PDs.

In the proposed IMSD algorithm, RS codes are decoded by the ABP-BM algorithm, where the ABP algorithm produces the extrinsic and the *a posteriori* probabilities of RS coded bits. The ABP algorithm is performed based on the code's binary parity-check matrix. For an (n, k_t) RS code, its parity-check matrix \mathbf{H}_t can be defined as

$$\mathbf{H}_t = \begin{bmatrix} 1 & \alpha & \cdots & \alpha^{n-1} \\ 1 & \alpha^2 & \cdots & \alpha^{2(n-1)} \\ \vdots & \vdots & \ddots & \vdots \\ 1 & \alpha^{n-k_t} & \cdots & \alpha^{(n-k_t)(n-1)} \end{bmatrix}. \quad (8)$$

Let \mathbf{A} further denote the companion matrix [27] of \mathbb{F}_{2^p} , which is a $p \times p$ binary matrix. The binary parity-check matrix \mathcal{H}_t of the RS code can be generated by replacing the entries α^ℓ of \mathbf{H}_t by \mathbf{A}^ℓ , where $\ell = 0, 1, \dots, 2^p - 2$.

III. ITERATIVE MULTISTAGE SOFT DECODING

Fig. 3 also shows the block diagram of the proposed IMSD algorithm. Let $P_{a,\text{DEM}}(c_j^{(t)})$, $P_{e,\text{DEM}}(c_j^{(t)})$ and $P_{p,\text{DEM}}(c_j^{(t)})$ denote the *a priori*, the extrinsic and the *a posteriori* probabilities of RS coded bit $c_j^{(t)}$ that are associated with the demapper, respectively. Similarly, let $P_{a,\text{DEC}}(c_j^{(t)})$, $P_{e,\text{DEC}}(c_j^{(t)})$ and $P_{p,\text{DEC}}(c_j^{(t)})$ denote the *a priori*, the extrinsic and the *a posteriori* probabilities of $c_j^{(t)}$ that are associated with the decoder, respectively. With the ABP-BM decoder, the BM algorithm estimates the RS coded bits. As a result, the deterministic probability $P_{d,\text{DEC}}(c_j^{(t)})$ can be obtained. That says if the level- t BM decoding succeeds, we obtain the coded bits estimations as $\hat{c}_0^{(t)}, \hat{c}_1^{(t)}, \dots, \hat{c}_{np-1}^{(t)}$. The deterministic probabilities of $c_j^{(t)}$ are $P_{d,\text{DEC}}(c_j^{(t)} = \hat{c}_j^{(t)}) = 1$ and $P_{d,\text{DEC}}(c_j^{(t)} = 1 - \hat{c}_j^{(t)}) = 0$.

The RS decoding consists of two stages. The ABP decoding yields both $P_{e,\text{DEC}}(c_j^{(t)})$ and $P_{p,\text{DEC}}(c_j^{(t)})$, where hard decision of $c_j^{(t)}$ will be made based on $P_{p,\text{DEC}}(c_j^{(t)})$. With a hard-decision received word, the BM algorithm decodes the message. If the level- t BM decoding succeeds, the decoder will feed back $P_{d,\text{DEC}}(c_j^{(t)})$. Otherwise, the extrinsic probability $P_{e,\text{DEC}}(c_j^{(t)})$ will be fed back. The decoding feedback provides the *a priori* information for the next level demapping. Decoding output of level $m-1$ ($P_{d,\text{DEC}}(c_j^{(m-1)})$ or $P_{e,\text{DEC}}(c_j^{(m-1)})$) will be fed back for the demapping at level 0. The next round multistage soft decoding starts. This iterative demapping-decoding will terminate when all levels are decoded or a predefined maximum number of global iterations (denoted as N_{GLO}) is reached. In the following, we will introduce the SISO demapping, the SISO decoding and their iterations. We will also introduce the complexity reducing approach.

A. SISO Demapping

The demapping and decoding are performed level-by-level for the MRS code. For example, demapping and decoding will be performed for level-0 RS code. Its decoding output will be utilized by the demapper of level 1. They form an multistage decoding process. In general, for level- t RS code, $P_{p,\text{DEM}}(c_j^{(t)})$ is determined by

$$P_{p,\text{DEM}}(c_j^{(t)} = \theta) = \sum_{s_i \in \mathcal{S}_{t,\theta}} P(y_j | s_i) P(s_i), \quad (9)$$

where $P(y_j | s_i)$ is the channel observation. The symbol probability $P(s_i)$ is determined by

$$P(s_i) = \prod_{t=0}^{m-1} P_{a,\text{DEM}}(c_j^{(t)} = [\mathcal{M}^{-1}(s_i)]_t). \quad (10)$$

Note that at the beginning, $P_{a,\text{DEM}}(c_j^{(t)} = 0) = P_{a,\text{DEM}}(c_j^{(t)} = 1) = 0.5, \forall (j, t)$. In order to constitute an iterative demapping-decoding mechanism, the coded bit's extrinsic probability is needed, which can be determined by

$$P_{e,\text{DEM}}(c_j^{(t)}) = \frac{P_{p,\text{DEM}}(c_j^{(t)})}{P_{a,\text{DEM}}(c_j^{(t)})}. \quad (11)$$

Based on (9)-(11), $P_{e,\text{DEM}}(c_j^{(t)})$ can be determined by

$$P_{e,\text{DEM}}(c_j^{(t)} = \theta) = \sum_{s_i \in \mathcal{S}_{t,\theta}} P(y_j | s_i) \prod_{t'=0, t' \neq t}^{m-1} P_{a,\text{DEM}}(c_j^{(t')} = [\mathcal{M}^{-1}(s_i)]_{t'}). \quad (12)$$

$P_{e,\text{DEM}}(c_j^{(t)})$ will be utilized by the following RS decoding.

B. SISO Decoding

For the level- t RS code, its SISO decoding starts with the following mapping

$$P_{e,\text{DEM}}(c_j^{(t)}) \mapsto P_{a,\text{DEC}}(c_j^{(t)}). \quad (13)$$

The *a priori* log-likelihood ratio (LLR) of bit $c_j^{(t)}$ can be determined by

$$L_a(c_j^{(t)}) = \ln \frac{P_{a,\text{DEC}}(c_j^{(t)} = 0)}{P_{a,\text{DEC}}(c_j^{(t)} = 1)}. \quad (14)$$

Subsequently, the *a priori* LLR vector of level- t RS code is

$$\underline{L}_a^{(t)} = [L_a(c_{j_0}^{(t)}), L_a(c_{j_1}^{(t)}), \dots, L_a(c_{j_{np-1}}^{(t)})]. \quad (15)$$

Entries of $\underline{L}_a^{(t)}$ will be sorted based on their magnitudes $|L_a(c_{j_t}^{(t)})|$, resulting in a refreshed index sequence $j_0, j_1, \dots, j_{(n-k_t)p-1}, \dots, j_{np-1}$. It indicates $|L_a(c_{j_0}^{(t)})| < |L_a(c_{j_1}^{(t)})| < \dots < |L_a(c_{j_{(n-k_t)p-1}}^{(t)})| < \dots < |L_a(c_{j_{np-1}}^{(t)})|$. Therefore, bits $c_{j_0}^{(t)}, c_{j_1}^{(t)}, \dots, c_{j_{(n-k_t)p-1}}^{(t)}$ are considered as the $(n-k_t)p$ least reliable bits, where their indices are collected in $\Theta_t = \{j_0, j_1, \dots, j_{(n-k_t)p-1}\}$ and $|\Theta_t| = (n-k_t)p$.

In order to perform the BP decoding, Gaussian elimination is needed in order to reduce the density of \mathcal{H}_t . This will be carried out based on the above sorting outcome. In \mathcal{H}_t , columns that are indexed by Θ_t will be reduced to weight-1, forming an $(n-k_t)p \times (n-k_t)p$ identity submatrix. Doing so, we can not only reduce the density of \mathcal{H}_t , but also minimize the propagation of the unreliable information during the BP decoding. Note that it is possible that not all of the $(n-k_t)p$ columns indexed by Θ_t can be reduced to weight-1. In this case, we can reduce columns $j_{(n-k_t)p}, j_{(n-k_t)p+1}$, and etc. The above process results in the adapted parity-check matrix \mathcal{H}'_t . We use $\tilde{\Theta}_t$ to denote the index set of the columns that have been reduced to weight-1 and $|\tilde{\Theta}_t| = (n-k_t)p$. If all columns that are indexed by Θ_t can be reduced to weight-1, $\tilde{\Theta}_t = \Theta_t$.

The following BP decoding will be performed based on \mathcal{H}'_t . Let h_{vj} denote the entry of \mathcal{H}'_t . We define

$$\mathbf{V}(j) = \{v | h_{vj} = 1, \forall 0 \leq v \leq (n-k_t)p - 1\}, \quad (16)$$

$$\mathbf{J}(v) = \{j | h_{vj} = 1, \forall 0 \leq j \leq np - 1\}. \quad (17)$$

The extrinsic LLR of $c_j^{(t)}$ is determined by

$$L_e(c_j^{(t)}) = \sum_{v \in \mathbf{V}(j)} 2 \tanh^{-1} \left(\prod_{j' \in \mathbf{J}(v) \setminus j} \tanh \left(\frac{L_a(c_{j'}^{(t)})}{2} \right) \right). \quad (18)$$

The *a posteriori* LLR of $c_j^{(t)}$ is further determined by

$$L_p(c_j^{(t)}) = L_a(c_j^{(t)}) + \eta L_e(c_j^{(t)}), \quad (19)$$

where $\eta \in (0, 1)$ is a damping factor. Note that although the Gaussian elimination has been performed, \mathcal{H}'_t remains dense for the BP decoding. It still contains many short circles that affect the reliability of the extrinsic information. Hence, η is needed to downgrade the extrinsic influence [26].

All RS coded bits $c_0^{(t)}, c_1^{(t)}, \dots, c_{np-1}^{(t)}$ can be estimated based on the *a posteriori* LLR vector

$$\underline{L}_p^{(t)} = [L_p(c_0^{(t)}), L_p(c_1^{(t)}), \dots, L_p(c_{np-1}^{(t)})]. \quad (20)$$

with the estimations, we can further obtain a received word $\underline{R}^{(t)}$, where $\underline{R}^{(t)} \in \mathbb{F}_{2^p}^n$. The BM decoding will be performed based on $\underline{R}^{(t)}$. If the BM decoding succeeds, $\hat{c}_j^{(t)}$ can be obtained and $P_{d,DEC}(c_j^{(t)})$ will be fed back to update $P_{a,DEM}(c_j^{(t)})$ by

$$P_{d,DEC}(c_j^{(t)}) \mapsto P_{a,DEM}(c_j^{(t)}). \quad (21)$$

Note that when the BM decoding succeeds, $P_{d,DEC}(c_j^{(t)})$ is more reliable than $P_{e,DEC}(c_j^{(t)})$ that is generated by the ABP algorithm. In this case, $P_{d,DEC}(c_j^{(t)})$ rather than $P_{e,DEC}(c_j^{(t)})$ would be fed back, providing more reliable information for the next level demapping. If the BM decoding fails, $P_{e,DEC}(c_j^{(t)})$ will be fed back to update $P_{a,DEM}(c_j^{(t)})$ by

$$P_{e,DEC}(c_j^{(t)}) \mapsto P_{a,DEM}(c_j^{(t)}). \quad (22)$$

Note that with $L_e(c_j^{(t)})$, $P_{e,DEC}(c_j^{(t)})$ can be obtained by

$$P_{e,DEC}(c_j^{(t)} = 0) = \frac{1}{1 + e^{-L_e(c_j^{(t)})}}, \quad (23)$$

$$P_{e,DEC}(c_j^{(t)} = 1) = \frac{1}{1 + e^{L_e(c_j^{(t)})}}. \quad (24)$$

The updated $P_{a,DEM}(c_j^{(0)}), P_{a,DEM}(c_j^{(1)}), \dots, P_{a,DEM}(c_j^{(t)})$ are used to calculate $P_{e,DEM}(c_j^{(t+1)})$ using (12) for the next level decoding. Note that if level- t RS code is decoded, it will not be processed in the next IMSD iteration.

It should be pointed out that the ABP algorithm is also iterative, implying there can be multiple Gaussian eliminations. In this case, $\underline{L}_p^{(t)}$ will be mapped to $\underline{L}_a^{(t)}$, triggering another round of sorting and Gaussian elimination. The decoding at level t will terminate either when the message is decoded or when the maximum number of ABP iteration (denoted as N_{ABP}) is reached. Each level RS decoding outcome can be validated by the maximum likelihood (ML) criterion [28].

C. CR-IMSD

The ABP-BM algorithm has a large decoding latency which is mainly caused by the Gaussian elimination. Our research has noticed that during the ABP decoding, the set of unreliable bits may not vary by a large portion. That says at level t , most of the $(n - k_t)p$ unreliable bits remain so at the next ABP iteration. This suggests we can use the existing matrix \mathcal{H}'_t without performing the Gaussian elimination. This helps

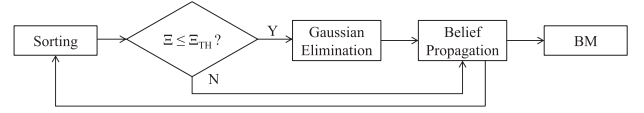


Fig. 4. The complexity reducing ABP-BM algorithm.

reduce the latency and complexity of the ABP-BM algorithm, further facilitating the IMSD for MRS codes. Fig. 4 shows the complexity reducing ABP-BM algorithm. Decoding each level RS code using this approach results in the CR-IMSD algorithm for the MRS codes.

Let $\tilde{\Theta}'_t$ denote the index set of columns that have been reduced to weight-1 in the previous ABP iteration. In the current ABP iteration, sorting the entries of $\underline{L}_a^{(t)}$ yields another index set Θ_t . Let Φ_t denote the number of common entries between $\tilde{\Theta}'_t$ and Θ_t . The overlapping portion between the two index sets can be defined as

$$\Xi_t = \frac{\Phi_t}{(n - k_t)p}, \quad (25)$$

where $0 \leq \Xi_t \leq 1$. We can further define an overlapping threshold Ξ_{TH} ($0 < \Xi_{TH} < 1$) in order to determine whether the Gaussian elimination needs to be performed. If $\Xi_t > \Xi_{TH}$, it implies there is a large portion of overlapping columns between $\tilde{\Theta}'_t$ and Θ_t . In this case, the Gaussian elimination can be skipped. The following BP decoding will be performed based on the existing matrix \mathcal{H}'_t . Otherwise, the Gaussian elimination will be performed, yielding a new adapted parity-check matrix \mathcal{H}'_t . Doing so, the IMSD process can be facilitated and this research shows its decoding performance penalty is marginal. Its performance-complexity tradeoff will be discussed in Section V-B.

IV. JOINT DESIGN OF CSK CONSTELLATION AND MRS CODE

This section looks into a joint design of CSK constellation and MRS code in order to optimize the decoding performance. The proposed CSK constellation design is based on the SP concept [29]. In order to optimize the IMSD performance, several designed SP constellations are further solicited based on maximizing the constellation's harmonic mean of MSED [30], [31]. Based on the designed CSK constellation, we will investigate different rules for designing MRS codes, including the capacity rule, the equal error probability rule and the balanced distances rule [32]–[34]. They all result in the HeMRS codes, realizing unequal error protection.

A. CSK Constellation Design

In order to introduce our design, the following definitions of CSK constellations are further needed. Consider an M -CSK constellation \mathcal{S} , it can be partitioned into m levels. At partitioning level t , we obtain a subset $\mathcal{S}(\theta_0 \cdots \theta_{t-1})$ as

$$\mathcal{S}(\theta_0 \cdots \theta_{t-1}) = \{s_i \mid [\mathcal{M}^{-1}(s_i)]_\tau = \theta_\tau, \forall 0 \leq \tau \leq t-1\}. \quad (26)$$

Let $D_t^{(0)}$ and $D_t^{(1)}$ denote the intraset MEDs of the subsets $\mathcal{S}(\theta_0 \cdots \theta_{t-1})$ and $\mathcal{S}(1\theta_1 \cdots \theta_{t-1})$ at the partitioning level t ,

TABLE I
MEDS OF DIFFERENT SP 16-CSK CONSTELLATIONS AT PARTITIONING LEVELS 0, 1 AND 2

SP constellation	Partitioning level t	$D_t^{(0)}$ and $D_t^{(1)}$	d_t
Type I	0	—	0.271893
	1	$D_1^{(0)} = 0.271897$, $D_1^{(1)} = 0.273119$	0.271897
	2	$D_2^{(0)} = 0.470933$, $D_2^{(1)} = 0.470933$	0.470933
Type II-V	0	—	0.271893
	1	$D_1^{(0)} = 0.470933$, $D_1^{(1)} = 0.271893$	0.271893
	2	$D_2^{(0)} = 0.470933$, $D_2^{(1)} = 0.470933$	0.470933

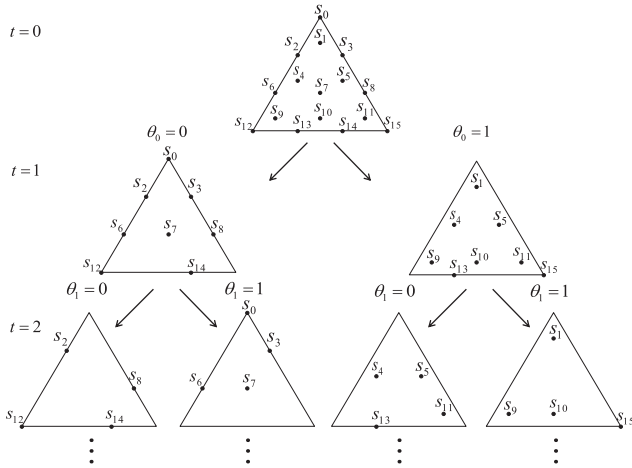


Fig. 5. SP process of a 16-CSK constellation.

respectively. They can be defined as

$$D_t^{(0)} = \min_{i \neq i'} \{ \|s_i - s_{i'}\|, \forall (s_i, s_{i'}) \in \mathcal{S}(0\theta_1 \cdots \theta_{t-1}) \text{ and } \forall \mathcal{S}(0\theta_1 \cdots \theta_{t-1}) \} \quad (27)$$

and

$$D_t^{(1)} = \min_{i \neq i'} \{ \|s_i - s_{i'}\|, \forall (s_i, s_{i'}) \in \mathcal{S}(1\theta_1 \cdots \theta_{t-1}) \text{ and } \forall \mathcal{S}(1\theta_1 \cdots \theta_{t-1}) \}. \quad (28)$$

Note that at partitioning level t , there are 2^{t-1} subsets $\mathcal{S}(0\theta_1 \cdots \theta_{t-1})$ and $\mathcal{S}(1\theta_1 \cdots \theta_{t-1})$, respectively. E.g., Fig. 5 shows the SP process of a 16-CSK constellation. When $t = 2$, we have $\mathcal{S}(00) = \{s_2, s_8, s_{12}, s_{14}\}$, $\mathcal{S}(01) = \{s_0, s_3, s_6, s_7\}$, $\mathcal{S}(10) = \{s_4, s_5, s_{11}, s_{13}\}$ and $\mathcal{S}(11) = \{s_1, s_9, s_{10}, s_{15}\}$. Furthermore, the intraset MED of partitioning level t is defined as

$$d_t = \min\{D_t^{(0)}, D_t^{(1)}\}. \quad (29)$$

Note that when $t = 0$, d_0 is the MED of the M -CSK constellation.

Based on the SP designing methodology, it is desirable to obtain $d_0 < d_1 < \cdots < d_{m-1}$ so that when an earlier level code is decoded, the following demapping performance can be enhanced thanks to a larger intraset MED. This will improve the performance of a multistage decoding mechanism. However, for an iterative scheme, it is also crucial to maximize the harmonic mean of the constellation's MSED, which is

defined as [31]

$$d_h^2 = \left(\frac{1}{m2^m} \sum_{t=0}^{m-1} \sum_{\theta=0}^1 \sum_{s_i \in \mathcal{S}_{t,\theta}} \frac{1}{\|s_i - s'_i\|^2} \right)^{-1}, \quad (30)$$

where s'_i is the constellation point whose demapping only differs from the demapping of s_i at bit t . Therefore, the proposed CSK constellation design has two stages. The SP design is first performed, resulting in several constellations that satisfy the criterion. Then, we will use d_h^2 as a criterion to choose one of the designs so that the iterative decoding performance can be maximized.

1) *Design Stage I:* Design the CSK constellation such that $d_0 \leq d_1 \leq \cdots \leq d_{m-1}$.

Fig. 5 shows the design of a 16-CSK constellation at partitioning levels 0, 1 and 2. Applying the SP criterion, it is intended to ensure a monotonically increasing intraset MED through the partition, i.e., $d_0 < d_1 < \cdots < d_{m-1}$. However, the CSK constellation's triangle shape makes it difficult to ensure $d_0 < d_1 < \cdots < d_{m-1}$. Our research has shown that strictly ensuring $d_0 < d_1 < \cdots < d_{m-1}$ would cause the intraset MEDs of level 1, $D_1^{(0)}$ and $D_1^{(1)}$, only slightly increase from the d_0 . This will limit the decoding performance at level 1. For example, Table I shows the MEDs of different SP 16-CSK constellations. Among them, Type I is designed based on $d_0 < d_1 < \cdots < d_{m-1}$. This results in $D_1^{(0)}$ and $D_1^{(1)}$ only slightly increase from the d_0 . However, relaxing the SP criterion and maintaining $d_0 \leq d_1 \leq \cdots \leq d_{m-1}$ will allow one of the intraset MEDs being remarkably increased at partitioning level 1. In Table I, Type II-V 16-CSK constellations are designed based on $d_0 \leq d_1 \leq \cdots \leq d_{m-1}$. It can be seen despite $d_0 = d_1$, $D_1^{(0)}$ is much larger than d_0 . This stage design yields multiple SP constellations. The labels of Type I-V SP constellations are shown in Table II, in which symbols s_0, \dots, s_{15} are denoted by their decimal labels $\varpi_0, \dots, \varpi_{15}$. The following Design Stage II will select a constellation that can maximize the iterative decoding performance.

2) *Design Stage II:* Based on the results of Stage I, choose a constellation that yields the largest d_h^2 .

Table II further gives d_h^2 of the five SP 16-CSK constellations that are obtained at Stage I. The IEEE standard constellation [3] is also given for reference. As shown in Table II, the IEEE standard 16-CSK constellation yields the smallest d_h^2 . This constellation is not designed for MRS codes that are equipped with iterative decoding. Among the five SP 16-CSK constellations, Type V yields the largest d_h^2 . Therefore, it will also yield a better iterative decoding

TABLE II
 d_h^2 OF DIFFERENT 16-CSK CONSTELLATIONS

	16-CSK symbols (s_0, s_1, \dots, s_{15})	d_h^2
IEEE Standard	(0, 1, 3, 5, 2, 7, 10, 6, 4, 11, 14, 13, 9, 15, 12, 8)	0.1327
SP, Type I	(14, 1, 8, 13, 2, 10, 4, 15, 7, 11, 9, 12, 6, 0, 5, 3)	0.4381
SP, Type II	(7, 13, 0, 5, 10, 8, 4, 6, 3, 14, 12, 11, 2, 9, 1, 15)	0.2836
SP, Type III	(7, 12, 1, 4, 10, 9, 5, 6, 2, 15, 13, 11, 3, 8, 0, 14)	0.3863
SP, Type IV	(6, 13, 1, 5, 10, 8, 4, 7, 2, 15, 12, 11, 3, 9, 0, 14)	0.4238
SP, Type V	(6, 12, 0, 5, 11, 9, 4, 7, 3, 14, 13, 10, 2, 8, 1, 15)	0.5061

performance in comparison with the others. Simulation results on this comparison will be given in Section V-D.

B. MRS Code Design

1) *Capacity Rule*: The MRS code design can be further performed based on the above designed CSK constellation. With the multilevel coding scheme, the transmission of a CSK symbol x_j over the physical channel can be separated into parallel transmission of m individual bits ($c_j^{(0)}, c_j^{(1)}, \dots, c_j^{(m-1)}$) over m equivalent channels ($0, 1, \dots, m-1$). We can analyze the capacity of each equivalent channel and design the code rate accordingly. Equipped with a competent decoding algorithm, more successful decoding of each component code can be achieved. This further enhances the overall IMSD performance.

Let $\mathcal{C}^{(t)}$ denote the capacity of equivalent channel t . For an m -level MRS coded transmission, the overall capacity \mathcal{C} is defined as

$$\mathcal{C} = \sum_{t=0}^{m-1} \mathcal{C}^{(t)}. \quad (31)$$

When $\mathcal{R}^{(t)} \leq \mathcal{C}^{(t)}$, error-free transmission of level- t RS code is possible. Let $X^{(t)}$ denote the transmitted variable at equivalent channel t and let Y denote the received variable. Using the multistage decoding, the capacity of equivalent channel t can be determined as the conditional mutual information $I(Y; X^{(t)} | X^{(0)} \dots X^{(t-1)})$.¹ Based on the chain rule of mutual information [35]

$$I(Y; X^{(0)} \dots X^{(m-1)}) = \sum_{t=0}^{m-1} I(Y; X^{(t)} | X^{(0)} \dots X^{(t-1)}), \quad (32)$$

the capacity of equivalent channel t can be determined by

$$\mathcal{C}^{(t)} = I(Y; X^{(t)} \dots X^{(m-1)} | X^{(0)} \dots X^{(t-1)}) - I(Y; X^{(t+1)} \dots X^{(m-1)} | X^{(0)} \dots X^{(t)}). \quad (33)$$

Let $\mathcal{C}(\mathcal{B})$ denote the channel capacity that is associated with a modulated symbol set \mathcal{B} . With the knowledge of bits $\theta_0, \dots, \theta_{t-1}$, we can define the symbol set $\mathcal{S}(\theta_0 \dots \theta_{t-1})$. Since $\theta_\tau \in \{0, 1\}$ and $0 \leq \tau \leq t-1$, there are 2^t permutations of $\theta_0 \dots \theta_{t-1}$. Hence, there are 2^t symbol sets $\mathcal{S}(\theta_0 \dots \theta_{t-1})$.

¹It is assumed that $I(Y; X^{(t)} | X^{(0)} \dots X^{(t-1)})$ is maximized by an appropriate distribution of $X^{(t)}$.

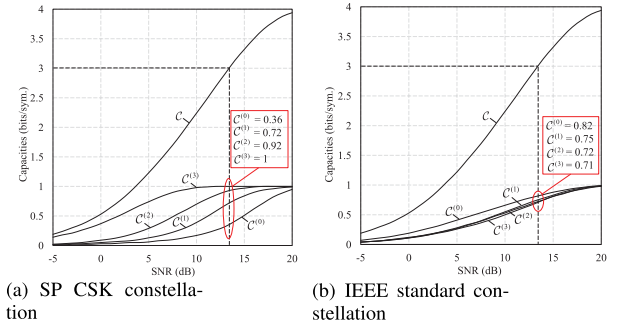


Fig. 6. The equivalent channel capacities of 16-CSK constellations.

Consequently, $I(Y; X^{(t)} \dots X^{(m-1)} | X^{(0)} \dots X^{(t-1)})$ can be determined by

$$I(Y; X^{(t)} \dots X^{(m-1)} | X^{(0)} \dots X^{(t-1)}) = \frac{1}{2^t} \sum_{\mathcal{S}(\theta_0 \dots \theta_{t-1})} \mathcal{C}(\mathcal{S}(\theta_0 \dots \theta_{t-1})). \quad (34)$$

Similarly,

$$I(Y; X^{(t+1)} \dots X^{(m-1)} | X^{(0)} \dots X^{(t)}) = \frac{1}{2^{t+1}} \sum_{\mathcal{S}(\theta_0 \dots \theta_t)} \mathcal{C}(\mathcal{S}(\theta_0 \dots \theta_t)). \quad (35)$$

Based on (33), we can determine the capacity of equivalent channel t by

$$\mathcal{C}^{(t)} = \frac{1}{2^t} \sum_{\mathcal{S}(\theta_0 \dots \theta_{t-1})} \mathcal{C}(\mathcal{S}(\theta_0 \dots \theta_{t-1})) - \frac{1}{2^{t+1}} \sum_{\mathcal{S}(\theta_0 \dots \theta_t)} \mathcal{C}(\mathcal{S}(\theta_0 \dots \theta_t)). \quad (36)$$

In particular, over the AWGN channel, capacity $\mathcal{C}(\mathcal{B})$ can be determined by

$$\mathcal{C}(\mathcal{B}) = \frac{1}{|\mathcal{B}|} \sum_{s_i \in \mathcal{B}} \int_{y_j} P(y_j | s_i) \log_2 \left(\frac{P(y_j | s_i)}{\frac{1}{|\mathcal{B}|} \sum_{s_\xi \in \mathcal{B}} P(y_j | s_\xi)} \right) dy_j, \quad (37)$$

in which it is assumed that each symbol of \mathcal{B} is equiprobable for transmission.

Consequently, we can design the level- t RS code by adjusting its code rate $\mathcal{R}^{(t)}$ based on the equivalent channel capacity $\mathcal{C}^{(t)}$. Fig. 6 shows the equivalent channel capacities of the 16-CSK constellations over the AWGN channel, where Fig.6(a) shows the capacities of the Type II-V designed SP

constellations and Fig.6(b) shows the capacities of the IEEE standard constellation. Labels of these constellations can be referred to Table II. Based on Fig.6(a), it can be seen that to achieve a channel capacity of 3 bits/sym., the equivalent channel capacities are $\mathcal{C}^{(0)} = 0.36$ bits/sym., $\mathcal{C}^{(1)} = 0.72$ bits/sym., $\mathcal{C}^{(2)} = 0.92$ bits/sym. and $\mathcal{C}^{(3)} = 1$ bit/sym., respectively. Therefore, to achieve the channel capacity, the designed SP 16-CSK constellations require to be incorporated with the HeMRS codes. For the IEEE standard 16-CSK constellation, to achieve $\mathcal{C} = 3$ bits/sym., $\mathcal{C}^{(0)}$, $\mathcal{C}^{(1)}$, $\mathcal{C}^{(2)}$ and $\mathcal{C}^{(3)}$ are similar as shown by Fig.6(b). It can be incorporated with HoMRS codes. The Section V-D will compare the performance of the above incorporations and demonstrate the merit of our design.

2) *Other Approaches*: Other multilevel code design approaches include the equal error probability rule [32]–[34], [36] and the balanced distance rule [32]. The design can also be done by analyzing the interplay between the demapping and the decoding using the EXIT function [19].

The equal error probability rule balances the performance of each level, so that each level contributes equally to the error probability of an MRS code. This can minimize the code's error probability. Let \mathcal{P} and \mathcal{P}_t denote the codeword error probability (CEP) of the MRS code and its level- t component code, respectively, and

$$\mathcal{P} = \sum_{t=0}^{m-1} \mathcal{P}_t. \quad (38)$$

\mathcal{P}_t can be estimated based on the union upper bound and the Euclidean distance enumerator. Given the level- t (n, k_t) RS code, the binary weight enumerator is defined as

$$\mathcal{W}_t(\mathcal{D}) = \sum_{\delta \geq \delta_{b,t}} w_{\delta,t} \mathcal{D}^\delta, \quad (39)$$

where $w_{\delta,t}$ is the multiplicity of level- t RS codewords with a binary weight of δ and $\delta_{b,t}$ is the average weight of the binary image of weight $(n - k_t + 1)$ RS codewords² [37]. The bound on \mathcal{P}_t can be tightened by the relevant Euclidean distance enumerator that is defined as

$$\mathcal{U}_t(\mathcal{Z}) = \sum_{\delta \geq \delta_{b,t}} w_{\delta,t} (\mathcal{Q}_t(\mathcal{Z}))^\delta, \quad (40)$$

where \mathcal{Q}_t is the average relevant constellation enumerator at level t [32]. The union upper bound \mathcal{P}_t can be written as

$$\begin{aligned} \mathcal{P}_t &\leq \mathcal{U}_t(e^{-\frac{1}{4N_0}}) \\ &= \sum_{\delta \geq \delta_{b,t}} w_{\delta,t} (\mathcal{Q}_t(e^{-\frac{1}{4N_0}}))^\delta, \end{aligned} \quad (41)$$

where N_0 is the noise power density spectrum of the channel.

Fig. 7 shows the upper bounds of the CEP of each component code when using the Type V SP 16-CSK over the AWGN channel. The component codes at levels 0, 1, 2 and 3 are the (63, 15), the (63, 45), the (63, 53) and the (63, 59) RS codes, respectively. The MRS coded transmission rate is 2.73 bits/sym.. It can be seen that CEP of each level is balanced at the CEP of 10^{-6} .

²Note that for the (n, k_t) RS code, the minimum weight of a nonzero codeword is $n - k_t + 1$.

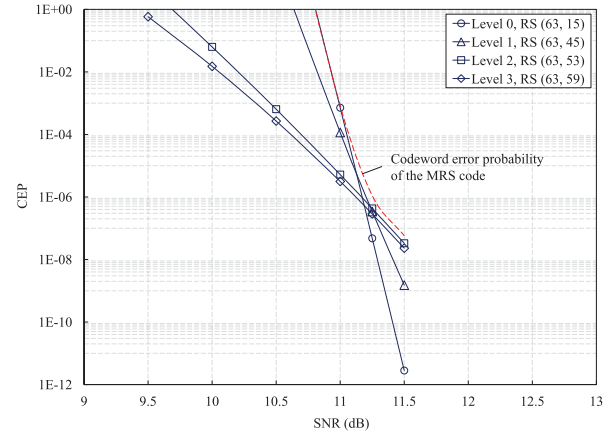


Fig. 7. Upper bounds of the CEP of each component code.

TABLE III
DESIGNED MRS CODES OF DIFFERENT RULES

Levels	Level 0	Level 1	Level 2	Level 3
Capacity rule	(63, 17)	(63, 37)	(63, 55)	uncoded
Equal error probability rule	(63, 15)	(63, 45)	(63, 53)	(63, 59)
Balanced distances rule	(63, 33)	(63, 33)	(63, 49)	(63, 57)

Using the balanced distances rule [32], the minimum Hamming distances are chosen to maintain $d_t^2(n - k_t + 1)$ equal for levels. For example, to maintain a coded transmission rate of 2.73 bits/sym., the balanced distances rule will lead to $\mathcal{R}^{(0)} = 0.53$ bits/sym., $\mathcal{R}^{(1)} = 0.53$ bits/sym., $\mathcal{R}^{(2)} = 0.78$ bits/sym. and $\mathcal{R}^{(3)} = 0.89$ bits/sym.. Employing the capacity rule, we can use Fig. 6(a) to determine $\mathcal{R}^{(0)} = 0.27$ bits/sym., $\mathcal{R}^{(1)} = 0.60$ bits/sym., $\mathcal{R}^{(2)} = 0.86$ bits/sym. and $\mathcal{R}^{(3)} = 1$ bit/sym.. Table III shows the component codes of the three designed HeMRS codes. All the design rules maintain the coded transmission rate of 2.73 bits/sym.. Performance of the three HeMRS codes will be compared in Section V-C.

V. SIMULATION RESULTS

We now show the decoding performance of MRS codes using the proposed IMSD algorithm. The simulation results are obtained over the AWGN channel. In our simulations, we let $N_{\text{ABP}} = 3$ and $\eta = 0.12$. Three BP iterations are performed based on each adapted matrix \mathcal{H}'_t . The decoding performance is evaluated in electronic SNR scale.

A. Performance of IMSD

Fig. 8 shows the BER performance of the HoMRS code that employs the (63, 47) RS codes as its component codes. The Type V SP 16-CSK constellation is employed. The proposed IMSD algorithm is compared with the conventional iterative multistage decoding (IMD) algorithm in which the RS decoding is performed by the BM algorithm. The conventional IMD iterates hard decoding estimations. It shows that the proposed IMSD algorithm significantly outperforms the conventional IMD algorithm. The decoding performance can be enhanced by increasing the maximum number of global iterations N_{GLO} . Without iterating soft information, the conventional IMD converges much earlier than the IMSD, yielding limited

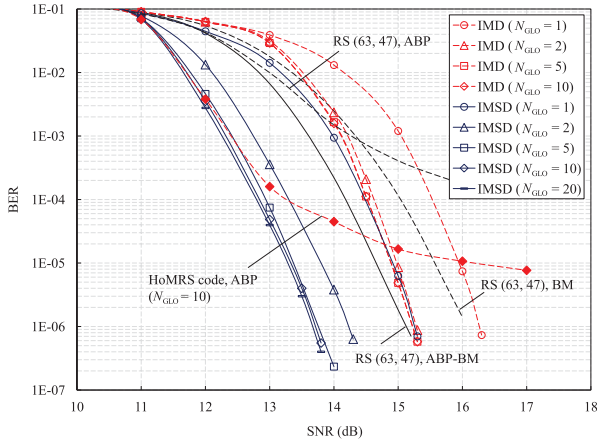


Fig. 8. Performance of the HoMRS code using 16-CSK over the AWGN channel.

iterative decoding gains. However, it should be pointed out that IMSD improves the decoding performance at the cost of its complexity. The ABP algorithm incurs extra complexity, including sorting, real number operation and binary operation. The real number operation and binary operation are caused by the BP decoding and the Gaussian elimination, respectively. As a result, the IMSD will have a larger decoding latency than the conventional IMD. For this, the CR-IMSD has been further proposed. Its performance-complexity tradeoff can be seen in the following subsection.

Fig. 8 also shows the performance of the HoMRS code in which its component codes are decoded by the ABP algorithm alone. It can be seen that using the ABP algorithm alone provides a rather poor performance, exhibiting an error floor. Despite the use of Gaussian elimination, there still exist too many short cycles in the adapted parity-check matrix. Hard-decisions made based on the *a posteriori* probabilities that are provided by the ABP algorithm will not be reliable. This can also be demonstrated by the ABP decoding performance of a single (63, 47) RS code, which is also shown in Fig. 8. Therefore, in decoding each component RS code, it is necessary to cascade the ABP and the BM algorithms. So that, advanced decoding performance of the MRS codes can be achieved.

In order to verify the advantage of MRS coded transmission, we also show the performance of a single (63, 47) RS code. The BM, ABP and ABP-BM decoding have been implemented for the code. It can be observed that without iteration, the HoMRS coded transmission performs worse than a signal RS code. This is because in the MRS coding scheme, m bits of m individual codes are bundled for transmission. If the channel introduces an error, this error may reside at all levels, degrading the performance. However, when the decoding starts to iterate, performance advantage of multilevel coding becomes remarkable.

B. Performance of CR-IMSD

Table IV highlights the BER difference of the CR-IMSD algorithm in decoding the above mentioned HoMRS code. It can be seen that by gradually decreasing the overlapping threshold Ξ_{TH} , the CR-IMSD algorithm will suffer a slight performance degradation. This is because decreasing the Ξ_{TH}

TABLE IV
BER OF THE CR-IMSD ALGORITHM

SNR (dB)	11	12	13
IMSD	7.08×10^{-2}	3.53×10^{-3}	4.85×10^{-5}
CR-IMSD ($\Xi_{TH} = 0.9$)	7.85×10^{-2}	5.43×10^{-3}	7.71×10^{-5}
CR-IMSD ($\Xi_{TH} = 0.8$)	7.86×10^{-2}	5.96×10^{-3}	9.50×10^{-5}
CR-IMSD ($\Xi_{TH} = 0.5$)	7.86×10^{-2}	6.33×10^{-3}	9.55×10^{-5}
CR-IMSD ($\Xi_{TH} = 0.3$)	7.86×10^{-2}	6.39×10^{-3}	9.55×10^{-5}

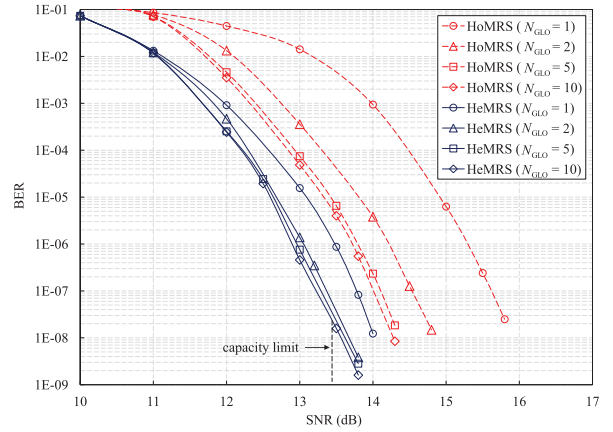


Fig. 9. Performance comparison between the HeMRS and the HoMRS codes using the SP 16-CSK.

will lead to less immediate parity-check matrix adaptations. The BP decoding output becomes less reliable. Table V further shows the average number of Gaussian eliminations in decoding an MRS code. Note that for the IMSD algorithm, there are at most $mN_{GLO}N_{ABP}$ Gaussian eliminations in decoding the HoMRS code. It can be seen that for both the IMSD algorithm and its complexity reducing variant, the average number of Gaussian eliminations reduces as the SNR increases. This is due to the succeed-and-exit decoding mechanism. By increasing the SNR, more reliable received information can be obtained. Consequently, less global iterations are needed to decode all codewords. Similarly, less ABP iterations will be needed to decode each component code. More importantly, Table V shows that the CR-IMSD can significantly reduce the number of Gaussian eliminations, especially when the $SNR \leq 12$ dB. This results in reducing the IMSD latency. Table V also shows that $\Xi_{TH} = 0.9$ and $\Xi_{TH} = 0.8$ yield a similar complexity reduction performance. However, Table IV shows $\Xi_{TH} = 0.9$ yields a noticeable performance advantage over the cases with $\Xi_{TH} < 0.9$. Therefore, for this MRS code, $\Xi_{TH} = 0.9$ yields a good performance-complexity tradeoff, which should be considered in practices.

C. Performance of HeMRS Codes

Fig. 9 compares the IMSD performance of the HeMRS and the HoMRS codes when employing the Type V SP 16-CSK constellation. The HeMRS code is designed based on the result of Fig. 6(a). To achieve an overall capacity of 3 bits/sym., its component codes at levels 0, 1 and 2 are the (63, 21), the (63, 45) and the (63, 57) RS codes, respectively, while level 3 is uncoded. To maintain a similar code rate,

TABLE V
AVERAGE NUMBER OF GAUSSIAN ELIMINATIONS WITH DIFFERENT OVERLAPPING THRESHOLDS

	N_{GLO}	SNR = 11 dB	SNR = 12 dB	SNR = 13 dB	SNR = 14 dB
IMSD	5	51	16	5	2
	10	98	19	5	2
CR-IMSD ($\Xi_{TH} = 0.9$)	5	18	7	3	1
	10	35	9	3	1
CR-IMSD ($\Xi_{TH} = 0.8$)	5	18	7	3	1
	10	35	8	3	1

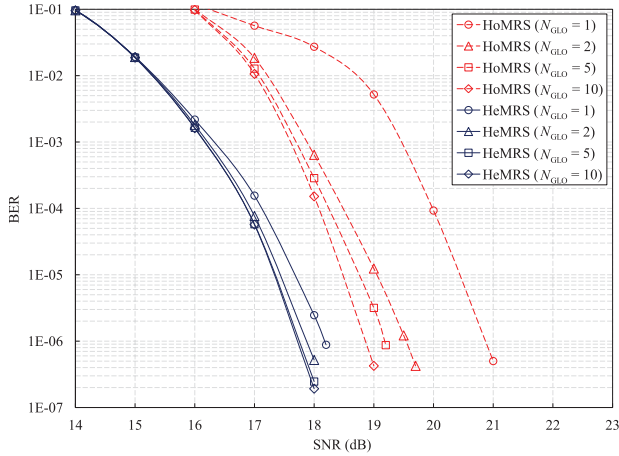


Fig. 10. IMSD performance of the HeMRS and the HoMRS codes using the SP 64-CSK.

the HoMRS code employs the (63, 47) RS codes as its component codes. It can be seen that the HeMRS code can significantly outperform its homogeneous counterpart. This indicates that by designing the code rate of each level according to the equivalent channel capacity, error-free transmission of each level can be ensured. This further benefits the overall IMSD performance. Fig. 6(a) shows that to realize a capacity of 3 bits/sym., an SNR of 13.4 dB is needed for the SP 16-CSK. Fig. 9 shows the performance of the designed HeMRS code is 0.3 dB away from the limit at the BER of 10^{-9} , demonstrating the effectiveness of our proposed IMSD message recovery scheme and the joint CSK-MRS design. Although we have chosen medium length RS codes as component codes, the IMSD algorithm can still yield a competent decoding performance. This is partly due to the fact that the ABP algorithm is more effective in decoding short-to-medium length RS codes. In comparison with long RS codes, there are less short cycles existing in their adapted parity-check matrices, making the ABP decoding more effective. As reported in [26], ABP-BM decoding of RS codes defined in \mathbb{F}_{64} could approach the code’s ML decoding lower bound.

Fig. 10 further shows the IMSD performance of the HeMRS and the HoMRS codes using the designed SP 64-CSK constellation. To achieve an overall capacity of 4.5 bits/sym., the equivalent channel capacity analysis shows $C^{(0)} = 0.15$ bits/sym., $C^{(1)} = 0.57$ bits/sym., $C^{(2)} = 0.79$ bits/sym., $C^{(3)} = 0.99$ bits/sym., $C^{(4)} = 1$ bit/sym. and $C^{(5)} = 1$ bit/sym., respectively. Hence, the HeMRS code’s component codes at levels 0, 1, 2 and 3 are the (63, 9), the (63, 35), the (63, 49) and the (63, 61) RS codes, respectively, while levels 4 and 5 are uncoded. The component codes of the HoMRS code are

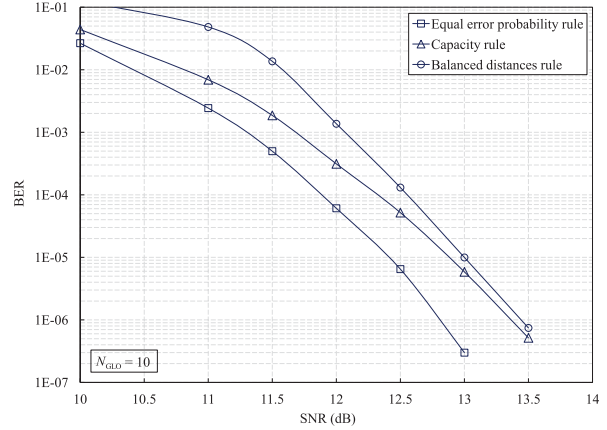


Fig. 11. Performance comparison of the HeMRS codes based on different design rules.

the (63, 47) RS codes. It again shows that the HeMRS code outperforms its homogeneous counterpart.

Fig. 11 further compares the performance of the three designed HeMRS codes of Table III, demonstrating the competency of different design rules. They all yield a coded transmission rate of 2.73 bits/sym.. It shows the equal error probability rule yields the best design. In comparison with the other two rules, it provides a more effective protection for level 0 of the multilevel coding scheme, which further contributes to a better overall performance. The HeMRS code designed by the balanced distances rule performs the worst. Based on Fig. 6(a), we know when the overall capacity is 2.73 bits/sym., $C^{(0)} = 0.27$ bits/sym.. The balanced distances rule leads to $\mathcal{R}^{(0)} > C^{(0)}$. Error-free transmission of level 0 cannot be ensured. However, it should be pointed out that despite its performance advantage, the equal error probability rule is less flexible in designing an MRS code. Unlike the capacity rule and balanced distances rule, it cannot be applied to design an MRS code with a given coded transmission rate. It requires a heuristic search on the component codes so that equal error probability of each component code can be reached.

D. Comparison of Different CSK Constellations

Based on the result of Fig. 6(b), we know that the IEEE standard 16-CSK constellation should be incorporated with a HoMRS code. Hence, Fig. 12 further shows the performance of this combination and compares it with the HeMRS code using the Type V SP 16-CSK. The HeMRS and the HoMRS codes are the same as those of Fig 9. It can be seen the HeMRS coding scheme yields a better decoding performance. We can also see that the IEEE standard constellation combined with the HoMRS code yields limited iterative decoding gains. The decoding performance of a single (63, 47) RS code with the

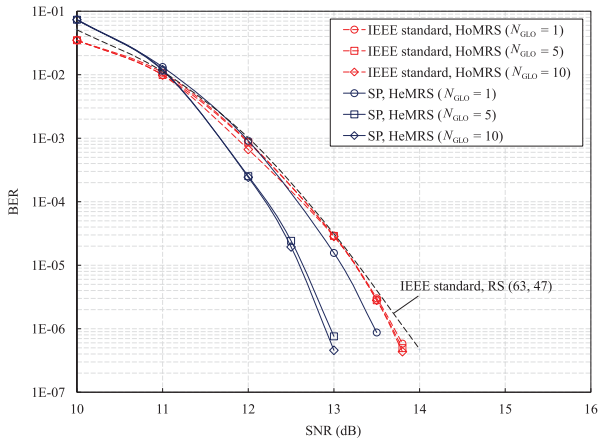


Fig. 12. Performance comparison between the HeMRS and the HoMRS codes using different constellations.

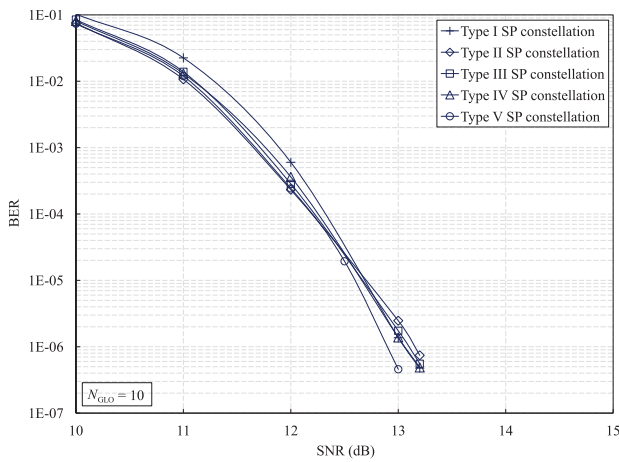


Fig. 13. Performance of different SP 16-CSK constellations over the AWGN channel.

IEEE standard 16-CSK constellation is also shown in Fig. 12. It can be seen that when using the IEEE standard constellation, the HoMRS code shows little performance improvement over a single code. It indicates that the IEEE standard 16-CSK constellation is not suitable for a multilevel coding scheme.

Finally, Fig. 13 shows the performance of using different designed SP 16-CSK constellations. The HeMRS code is the same as the one of Fig. 9. Table I shows that Type I is different from Types II–V at Stage I constellation design as it strictly requires the intraset MED to be monotonically increasing. Fig. 13 shows Type I yields a relatively poor iterative decoding performance. This is because Type I design results in the intraset MED of the subset only a slight increase from level 0 to level 1, limiting the multistage decoding performance. Table II shows that Type V SP constellation yields the largest d_h^2 . Fig. 13 verifies its iterative decoding performance advantage over other SP constellations when the SNR is greater than 12.2 dB. In contrast, Type II SP constellation yields the smallest d_h^2 . Consequently, it yields the worst iterative decoding performance at high SNR region. These results verify that besides the SP criterion, maximizing the harmonic mean of the constellation's MSED is also important to optimize the iterative decoding performance.

VI. CONCLUSIONS

This paper has proposed the MRS coded transmission for VLC, realizing spectrally efficient transmission. An IMSD algorithm for MRS codes has been proposed to maximize its error-correction performance. Each level RS decoding is realized by the ABP-BM algorithm, delivering either the extrinsic or the deterministic probabilities for the coded bits. Over the multistage decoding, the earlier level decoding events help the later ones by providing better *a priori* information. A CR-IMSD algorithm has been further proposed to reduce the decoding latency. Moreover, we have proposed a joint design of CSK constellation and MRS code. The CSK constellation design has two stages, considering both the SP criterion and the harmonic mean of the constellation's MSED. Different design rules for MRS code design have been investigated. The capacity rule is recommended by considering its design flexibility and effectiveness. Finally, our simulation results have vindicated that the proposed IMSD algorithm by showing it achieves a remarkable performance gain over the existing decoding algorithm. The joint design of CSK constellation and MRS code can further enhance the performance. The HeMRS code designed by the capacity rule that performs only 0.3 dB away from the limit at the BER of 10^{-9} .

REFERENCES

- [1] D. Karunatilaka, F. Zafar, V. Kalavally, and R. Parthiban, "LED based indoor visible light communications: State of the art," *IEEE Commun. Surveys Tuts.*, vol. 17, no. 3, pp. 1649–1678, 3rd Quart., 2015.
- [2] P. H. Pathak, X. Feng, P. Hu, and P. Mohapatra, "Visible light communication, networking, and sensing: A survey, potential and challenges," *IEEE Commun. Surveys Tuts.*, vol. 17, no. 4, pp. 2047–2077, 4th Quart., 2015.
- [3] *IEEE Standard for Local and Metropolitan Area Networks—Part 15.7: Short-Range Wireless Optical Communication Using Visible Light*, IEEE Standard 802.15.7, Sep. 2011, pp. 1–309.
- [4] R. J. Drost and B. M. Sadler, "Constellation design for color-shift keying using billiards algorithms," in *Proc. IEEE Globecom Workshops*, Miami, FL, USA, Dec. 2010, pp. 980–984.
- [5] R. J. Drost and B. M. Sadler, "Constellation design for channel pre-compensation in multi-wavelength visible light communications," *IEEE Trans. Commun.*, vol. 62, no. 6, pp. 1995–2005, Jun. 2014.
- [6] E. Monteiro and S. Hranilovic, "Design and implementation of color-shift keying for visible light communications," *J. Lightw. Technol.*, vol. 32, no. 10, pp. 2053–2060, May 15, 2014.
- [7] Y. Chen, M. Jiang, L. Zhang, and X. Chen, "Polarity modulated complex colour shift keying for OFDM-based visible light communication," in *Proc. IEEE/CIC Int. Conf. Commun. China (ICCC)*, Qingdao, China, Oct. 2017, pp. 1–5.
- [8] R. Singh, T. O'Farrell, and J. P. R. David, "An enhanced color shift keying modulation scheme for high-speed wireless visible light communications," *J. Lightw. Technol.*, vol. 32, no. 14, pp. 2582–2592, Jul. 15, 2014.
- [9] R. Singh, T. O'Farrell, and J. P. R. David, "Higher order colour shift keying modulation formats for visible light communications," in *Proc. IEEE Veh. Technol. Conf. (VTC)*, Glasgow, U.K., May 2015, pp. 1–5.
- [10] Y. Chen and M. Jiang, "Joint colour-and-spatial modulation aided visible light communication system," in *Proc. IEEE Veh. Technol. Conf. (VTC)*, Nanjing, China, May 2016, pp. 1–5.
- [11] C. Zhu *et al.*, "Hierarchical colour-shift-keying aided layered video streaming for the visible light downlink," *IEEE Access*, vol. 4, pp. 3127–3152, 2016.
- [12] R. Singh, T. O'Farrell, and J. P. R. David, "Analysis of forward error correction schemes for colour shift keying modulation," in *Proc. IEEE 26th Ann. Int. Symp. Pers., Indoor, Mobile Radio Commun. (PIMRC)*, Hong Kong, China, Aug./Sep. 2015, pp. 575–579.
- [13] L. M. Hwang, Y. W. Kim, B. G. Choi, and K. S. Kim, "Performance of color shift keying-space time block code-orthogonal frequency division multiplexing system on visible light communication," in *Proc. Int. Conf. Syst. Inform. (ICSAI)*, Shanghai, China, Nov. 2014, pp. 602–606.

- [14] J. Jiang, R. Zhang, and L. Hanzo, "Analysis and design of three-stage concatenated color-shift keying," *IEEE Trans. Veh. Technol.*, vol. 64, no. 11, pp. 5126–5136, Nov. 2015.
- [15] Z. Babar *et al.*, "Reduced-complexity iterative receiver for improving the IEEE 802.15.7 convolutional-coded color shift keying mode," *IEEE Commun. Lett.*, vol. 21, no. 9, pp. 2005–2008, Sep. 2017.
- [16] H. Imai and S. Hirakawa, "A new multilevel coding method using error-correcting codes," *IEEE Trans. Inf. Theory*, vol. IT-23, no. 3, pp. 371–377, May 1977.
- [17] P. A. Martin and D. P. Taylor, "On multilevel codes and iterative multistage decoding," *IEEE Trans. Commun.*, vol. 49, no. 11, pp. 1916–1925, Nov. 2001.
- [18] M. Isaka and H. Imai, "On the iterative decoding of multilevel codes," *IEEE J. Sel. Areas Commun.*, vol. 19, no. 5, pp. 935–943, May 2001.
- [19] Y. Wang and A. G. Burr, "Code design for iterative decoding of multilevel codes," *IEEE Trans. Commun.*, vol. 63, no. 7, pp. 2404–2419, Jul. 2015.
- [20] J. Massey, "Shift-register synthesis and BCH decoding," *IEEE Trans. Inf. Theory*, vol. IT-15, no. 1, pp. 122–127, Jan. 1969.
- [21] E. M. Husni, "Reed Solomon coded MPSK modulation for a Gaussian channel," in *Proc. Int. Conf. Instrum., Commun., Inf. Technol., Biomed. Eng.*, Bandung, Indonesia, Nov. 2009, pp. 1–5.
- [22] E. M. Husni and P. Sweeney, "Robust Reed Solomon coded MPSK modulation," *J. ICT Res. Appl.*, vol. 4, no. 2, pp. 95–113, 2010.
- [23] S. Y. Chung and H.-L. Lou, "Multilevel RS/convolutional concatenated coded QAM for hybrid IBOC-AM broadcasting," *IEEE Trans. Broadcast.*, vol. 46, no. 1, pp. 49–59, Mar. 2000.
- [24] A. Vardy and Y. Be'ery, "Bit-level soft-decision decoding of Reed–Solomon codes," *IEEE Trans. Commun.*, vol. 39, no. 3, pp. 440–444, Mar. 1991.
- [25] V. Ponnampalam and B. Vucetic, "Soft decision decoding of Reed–Solomon codes," *IEEE Trans. Commun.*, vol. 50, no. 11, pp. 1758–1768, Nov. 2002.
- [26] J. Jiang and K. R. Narayanan, "Iterative soft-input soft-output decoding of reed–solomon codes by adapting the parity-check matrix," *IEEE Trans. Inf. Theory*, vol. 52, no. 8, pp. 3746–3756, Aug. 2006.
- [27] R. Horn and C. Johnson, *Matrix Analysis*. New York, NY, USA: Cambridge Univ. Press, 1985.
- [28] T. Kaneko, T. Nishijima, H. Inazumi, and S. Hirasawa, "An efficient maximum-likelihood-decoding algorithm for linear block codes with algebraic decoder," *IEEE Trans. Inf. Theory*, vol. 40, no. 2, pp. 320–327, Mar. 1994.
- [29] G. Ungerboeck, "Channel coding with multilevel/phase signals," *IEEE Trans. Inf. Theory*, vol. IT-28, no. 1, pp. 55–67, Jan. 1982.
- [30] A. Chindapol and J. A. Ritcey, "Design, analysis, and performance evaluation for BICM-ID with square QAM constellations in rayleigh fading channels," *IEEE J. Sel. Areas Commun.*, vol. 19, no. 5, pp. 944–957, May 2001.
- [31] X. Li, A. Chindapol, and J. A. Ritcey, "Bit-interleaved coded modulation with iterative decoding and 8 PSK signaling," *IEEE Trans. Commun.*, vol. 50, no. 8, pp. 1250–1257, Aug. 2002.
- [32] U. Wachsmann, R. F. H. Fischer, and J. B. Huber, "Multilevel codes: Theoretical concepts and practical design rules," *IEEE Trans. Inf. Theory*, vol. 45, no. 5, pp. 1361–1391, Jul. 1999.
- [33] U. Wachsmann and J. B. Huber, "Distance profile of multilevel coded transmission and rate design," in *Proc. Inf. Theory Workshop (ITW)*, Killarney, Ireland, Jun. 1998, pp. 10–11.
- [34] J. Huber and L. F. Nachrichtentechnik, "Multilevel codes: Distance profiles and channel capacity," in *Proc. ITG-Fachbericht Conf. Rec.*, Germany, Oct. 1994, pp. 305–319.
- [35] T. M. Cover and J. A. Thomas, *Elements of Information Theory*. Hoboken, NJ, USA: Wiley, 2003.
- [36] A. G. Burr and T. J. Lunn, "Block-coded modulation optimized for finite error rate on the white Gaussian noise channel," *IEEE Trans. Inf. Theory*, vol. 43, no. 1, pp. 373–385, Jan. 1997.
- [37] M. El-Khamy and R. J. McEliece, "Bounds on the average binary minimum distance and the maximum likelihood performance of Reed Solomon codes," in *Proc. 42nd Allerton Conf. Commun., Control, Comput.*, Oct. 2004, pp. 290–299.



Xin Huang received the B.Sc. degree in communication engineering from Jinan University, Guangzhou, China, in 2016. She is currently pursuing the M.Sc. degree in information and communication engineering with Sun Yat-sen University, Guangzhou. Her research interests include channel coding and wireless communications.



Li Chen (S'07–M'08–SM'14) received the B.Sc. degree in applied physics from Jinan University, China, in 2003, and the M.Sc. degree in communications and signal processing and the Ph.D. degree in communications engineering from Newcastle University, U.K., in 2004 and 2008, respectively. From 2007 to 2010, he was a Research Associate with Newcastle University. In 2010, he was a Lecturer with the School of Information Science and Technology, Sun Yat-sen University, China, where he became an Associate Professor in 2011. From 2011 to 2012, he was an occasional Visiting Scholar with the Institute of Network Coding, The Chinese University of Hong Kong. In 2015, he was a Visitor with the Institute of Communication Engineering, Ulm University, Germany. From 2015 to 2016, he was a Visiting Associate Professor with the Department of Electrical Engineering, University of Notre Dame, USA. Since 2016, he has been a Professor with the School of Electronics and Communication Engineering, Sun Yat-sen University, where he is currently a Deputy Dean of the School. His primary research interests include information theory, channel coding, and data communications. He is a member of the Conference Committee of the IEEE Information Theory Society and the Chinese Information Theory Society. He is a Senior Member of the Chinese Institute of Electronics. He has been a technical program committee (TPC) member of various international conferences. He was a recipient of the British Overseas Research Scholarship and the Chinese Information Theory Young Researcher Award in 2014. As a General Co-Chair, he has hosted the 2018 IEEE Information Theory Workshop (ITW) at Guangzhou. He has been a Principle Investigator for three National Natural Science Foundation of China projects and a Co-Investigator of the National Basic Research Program (973 Program) Project. He is an Associate Editor of the IEEE TRANSACTIONS ON COMMUNICATIONS.



Wenjun Chen received the B.Eng. degree in electronic information science and technology from Sun Yat-sen University, Guangzhou, China, in 2017, where he is currently pursuing the M.Eng. degree in information and communication engineering. His research interests include visible light communication and underwater wireless optical communication.



Ming Jiang (M'07–SM'13) received the B.Eng. and M.Eng. degrees from the South China University of Technology (SCUT), China, and the Ph.D. degree from the University of Southampton, U.K., all in electronic engineering. He has substantial international and industrial experience with Fortune 500 telecom companies. From 2006 to 2013, he has held key research and development and/or management positions at the Samsung Electronics Research Institute (SERI), U.K., the Nortel Networks' Research and Development Centre, China, and telecom equipment maker New Postcom, China, where he actively participated in numerous collaborative projects, including European FP6 WINNER-II, European FP7 DAVINCI, Mobile WiMAX (IEEE802.16m), and 3GPP LTE/LTE-A standardization across European Union, North America, and Asia, researching and designing novel algorithms, telecommunication standards, and radio access and core network products. Since 2013, he has been a Full Professor and a Ph.D. Supervisor with Sun Yat-sen University, China, where he is involved in scientific research and technology transfer with industrial partners. He has co-authored or contributed to 5 Wiley books, more than 50 papers in prestigious international journals and conferences, more than 50 patents, and more than 400 LTE/LTE-A/WiMAX standardization contributions. His research interests fall into next-generation wireless mobile communications, including VLC, MIMO, OFDM, D2D, and HetNets. He was a recipient of several Chinese Council Awards in 2011, including Innovative Leading Talents, Outstanding Experts, and Top Overseas Scholars.